

# UC Berkeley

## UC Berkeley Previously Published Works

### Title

Entropy is an important design principle in the photosystem II supercomplex.

### Permalink

<https://escholarship.org/uc/item/8kx2999d>

### Journal

Proceedings of the National Academy of Sciences of the United States of America,  
122(12)

### Authors

Hall, Johanna

Yang, Shiun-Jr

Limmer, David

et al.

### Publication Date

2025-03-25

### DOI

10.1073/pnas.2426331122

Peer reviewed



# Entropy is an important design principle in the photosystem II supercomplex

Johanna L. Hall<sup>a,b,c</sup>, Shiun-Jr Yang<sup>a,b,c,1</sup>, David T. Limmer<sup>a,c,d,e</sup>, and Graham R. Fleming<sup>a,b,c,2</sup>

Affiliations are included on p. 6.

Edited by Robert Blankenship, Washington University in St. Louis, St. Louis, MO; received December 16, 2024; accepted February 18, 2025 by Editorial Board Member Peter J. Rossky

Photosystem II (PSII) can achieve near-unity quantum efficiency of light harvesting in ideal conditions and can dissipate excess light energy as heat to prevent the formation of reactive oxygen species (ROS) under light stress. Understanding how this pigment–protein complex accomplishes these opposing goals is a topic of great interest that has so far been explored primarily through the lens of the system energetics. Despite PSII's known flat energy landscape, a thorough consideration of the entropic effects on energy transfer in PSII is lacking. In this work, we aim to discern the free energetic design principles underlying the PSII energy transfer network. To accomplish this goal, we employ a structure-based rate matrix and compute the free energy terms in time following a specific initial excitation to discern how entropy and enthalpy drive ensemble system dynamics. We find that the interplay between the entropy and enthalpy components differ among each protein subunit, which allows each subunit to fulfill a unique role in the energy transfer network. This individuality ensures that PSII can accomplish efficient energy trapping in the reaction center (RC), effective nonphotochemical quenching (NPQ) in the periphery, and robust energy trapping in the other-monomer RC if the same-monomer RC is closed. We also show that entropy, in particular, is a dynamically tunable feature of the PSII free energy landscape accomplished through regulation of LHCII binding. These findings help rationalize natural photosynthesis and provide design principles for more efficient solar energy harvesting technologies.

free energy | entropy | energy landscape | ensemble dynamics | excitation energy transfer

Photosystem II of land plants and other oxygenic photosynthetic organisms possesses the unique ability to split water and generate molecular oxygen. The reaction center (RC), where charge separation is initiated, is coupled to an antenna containing several hundred chlorophyll (Chl) molecules to optimize photosynthetic yield in varying light levels. This pigment–protein supercomplex can convert harvested light energy into a charge separation with near-perfect quantum efficiency (1–3). In light stress conditions, Photosystem II (PSII) is able to dissipate excess light energy as heat to prevent the formation of reactive oxygen species (ROS) via reaction of molecular oxygen with the chlorophyll triplet excited state (4–6). Many of the photoprotective capabilities are hypothesized to take place in the periphery of PSII because of the high oxidative potential of the RC components (7–10), which limits the ability to place photoprotective molecules close to the RC. In this study, we explore how entropic driving forces facilitate these opposing design requirements of PSII.

Perhaps the most intuitive design for an antenna/RC system is that of an energy funnel with the RC located at the energy minimum. Indeed this is precisely the approach adopted by the purple bacterial B800/B850/RC system, for example (1, 11). PSII, however, has a multi-subunit construction with the lowest energy levels of all the subunits having very similar energies (1) (*SI Appendix, Fig. S1*). This has led to descriptions of the PSII antenna system as a flat landscape (12, 13), as a very shallow funnel (14, 15), or as lacking a funnel (16–18). This, in turn, raises the question of the driving force for energy transfer to the RC and the potential role of entropic in addition to enthalpic contributions. The availability of high-resolution structures for the 204 Chl-containing C<sub>2</sub>S<sub>2</sub>-type and 312 Chl C<sub>2</sub>S<sub>2</sub>M<sub>2</sub>-type dimeric supercomplexes (19, 20), along with quantitative models for the excitation dynamics for both structures (12, 13), allows us to explore the free energy landscape of the supercomplexes. Here, we use these dynamical models to study the stochastic thermodynamics accompanying photorelaxation and quantify the time-dependent changes to both the energy and entropy. These ensemble-level calculations give insight into the evolution of the initial exciton and we

## Significance

The free energy landscape of light harvesting systems is a key feature dictating energy transfer dynamics and overall system efficiency. Understanding the design components of the free energy landscape and how to manipulate them is crucial for constructing synthetic light-harvesting systems that efficiently generate renewable energy or optimizing natural light-harvesting systems to increase biomass production. Previous research has largely focused on the energy landscape of light-harvesting systems. Here, we analyze the full free energy equation in Photosystem II ensemble dynamics to understand its impressive quantum efficiency. We demonstrate the importance of the entropy and define a framework to characterize its role in the energy transfer network, which can be applied to the synthesis of more efficient systems.

Preprint server: A preprint version of this article is available on arXiv (<https://doi.org/10.48550/arXiv.2412.12418>).

Author contributions: J.L.H. designed research; J.L.H. performed research; J.L.H. and S.-J.Y. contributed new reagents/analytic tools; J.L.H., S.-J.Y., D.T.L., and G.R.F. analyzed data; and J.L.H., S.-J.Y., D.T.L., and G.R.F. wrote the paper.

The authors declare no competing interest.

This article is a PNAS Direct Submission. R.B. is a guest editor invited by the Editorial Board.

Copyright © 2025 the Author(s). Published by PNAS. This open access article is distributed under [Creative Commons Attribution License 4.0 \(CC BY\)](https://creativecommons.org/licenses/by/4.0/).

<sup>1</sup>Present address: Department of Chemistry, Massachusetts Institute of Technology, Cambridge, MA 02139.

<sup>2</sup>To whom correspondence may be addressed. Email: [grfleming@lbl.gov](mailto:grfleming@lbl.gov).

This article contains supporting information online at <https://www.pnas.org/lookup/suppl/doi:10.1073/pnas.2426331122/-/DCSupplemental>.

Published March 19, 2025.

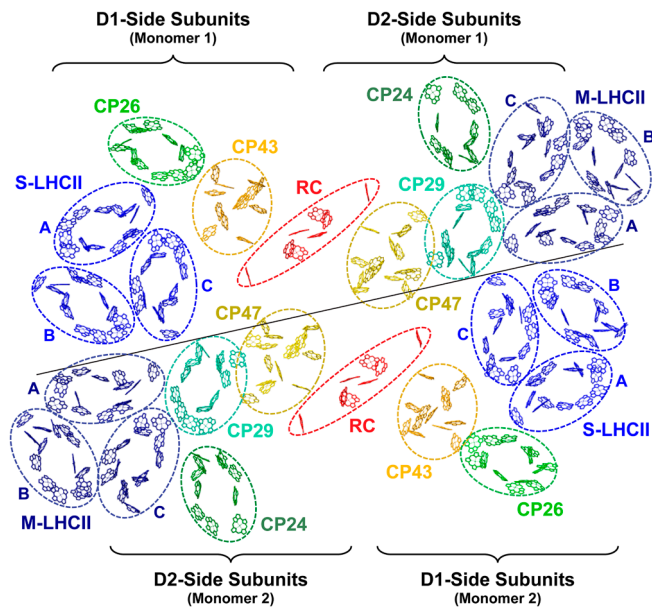


**Fig. 1.** The pigment arrangement of the  $C_2S_2M_2$ -type PSII supercomplex with protein subunits labeled (PDB: 5XNL) (20). The solid line marks the separation of the two monomers.

find that, qualitatively, the ensemble evolution can be thought of in two phases. First, an entropic exploration of the landscape distributes population among the chromophores with similar energies. Second, a more directed motion takes population down the shallow energy gradient toward the RC. We also show that when one of the two RCs is closed through prior excitation, the entropic phase on the side of the dimeric structure with a closed RC is elongated, allowing more time for the excitation to find the second, open, RC. We also show how the entropy component of the free energy landscape is a tunable parameter, which PSII can alter by regulating the binding of peripheral antenna complexes (21–26). These calculations provide insight into how the design of the PSII supercomplex enables the combination of both efficient charge separation and effective photoprotection and how these design principles can be applied to the construction and characterization of general energy harvesting systems.

## Methods

**Rate Matrix Construction.** We employ a structure-based quantum dynamical-rate matrix  $K$ , where element  $k_{ij}$  describes the energy transfer rate from exciton state  $j$  to state  $i$  in units of [ $\text{ps}^{-1}$ ]. The rate matrix for the  $C_2S_2M_2$  PSII supercomplex was constructed from the 5XNL structure of *Pisum sativum* (20) (Fig. 1) and the  $C_2S_2$  rate matrix was constructed from the 3JCU structure of *Spinacia oleracea* (19) (SI Appendix, Fig. S2), as well as from available Hamiltonians for the protein subunits (27–31). The rates were quantified by organizing the Chl molecules into domains based on coulombic coupling strength and degree of exciton delocalization, then applying Modified Redfield Theory for intradomain transfer and Generalized Forster Theory for interdomain transfer (16, 32) (SI Appendix). Based on the inhomogeneous broadening widths reported in the literature, a random number is added to the site energy of each chlorophyll and 500 sets of site energies are generated to construct 500 rate matrices. The calculation of entropy is based on the averaged rate matrix from these 500 realizations. We justify the use of the averaged rates based on Amarnath et al.'s finding that the averaged rate matrix produces the same fluorescence decay dynamics as the average of the result from each individual rate matrix (33). The rates satisfy detailed balance with respect to a Boltzmann distribution of each excitonic state, which allows for its thermodynamic interpretation (34). Unless otherwise specified, calculations are performed with the  $C_2S_2M_2$  rate matrix at 300K.

**Free Energy Calculations.** Following an excitation, where the initial condition is defined as a single exciton or linear combination of sites in the PSII supercomplex, we evolve the population vector,  $P(t) = \{p_1(t), p_2(t) \dots\}$ , using the direct integration of the master equation,

$$P(t) = e^{Kt}P(0), \quad [1]$$

where  $p_i(t)$  is the probability that the  $i$ th exciton state is excited. The probability of the excitation following a specific trajectory is proportional to the energy transfer rates between each state in the trajectory. Thus, the rate matrix accounts for the relative probability of the trajectories in the ensemble.

Entropy was calculated using the Shannon entropy  $\langle S(t) \rangle = -k_B \sum_i p_i(t) \ln p_i(t)$  and enthalpy was calculated from the energy levels of each state  $\langle H(t) \rangle = \sum_i p_i(t) E_i(t)$ . The entropic and enthalpic components of the free energy are computed following

$$\Delta G(t) = \Delta H(t) - T\Delta S(t), \quad [2]$$

where we define  $\Delta H(t) = \langle H(t) \rangle - H(0)$  as the enthalpy change and  $\Delta S(t) = \langle S(t) \rangle - S(0)$  as the entropy change, relative to their initial conditions. Because we are working in the exciton basis, we define an excitation of Chl  $a$  509 in CP43, for example, as the exciton state that is most localized in that chlorophyll. We model open RCs by adding an irreversible trap in the RC of each dimer using phenomenological rates. Although adding irreversible trap states breaks detailed balance, there still exists a well-defined trajectory ensemble whose dynamics evolve in a thermodynamically consistent way. The time evolution of the enthalpy and entropy we report are interpretable as that consistent with a constraint of ending at the RC. We define the location of the trap as the midpoint between the RC Pheo $_{D1}$  (pheophytin) and Chl $_{D1}$  molecules, which are predicted to form the charge transfer state (35) that we set as the lowest-energy state in the RC. To compute the distance of pigments from the open RC, we use the three-dimensional coordinates, determined from the structure, of the central Mg atom for chlorophyll and the approximate center of the porphyrin ring for pheophytin.

The enthalpy change describes both the scale and directionality (uphill or downhill) of the ensemble-averaged energy change of an exciton at specific times in the dynamics resulting from a defined initial condition. If the enthalpy maximum occurs after time zero, this point reveals the time before which the average population transfers against an energy gradient and after which the ensemble follows downhill excitation energy transfer (EET) to the RC trap. If the enthalpy change is negative, then the dynamics are driven by the availability of downhill energy transfer steps.

The entropy change, on the other hand, characterizes the spatial distribution of the ensemble EET trajectories at a given time. If the entropy increases, then ensemble energy transfer is driven by a high accessibility of nearby states. While the entropy is increasing, the ensemble population continues to spread out, reflective of individual trajectories following more divergent EET pathways. Likewise, when the entropy decreases, the ensemble of excitations becomes more directed and follows increasingly common pathways. Therefore, the time when the entropy is at a maximum is referred to as the population contraction time.

## Simulation Results and Discussion

The entropic and enthalpic components of the free energy change are plotted in Fig. 2. An example of the full  $\Delta G$  curve can be found in SI Appendix, Fig. S10. As entropy increases, the plotted entropy component,  $-T\Delta S(t)$ , decreases, so the minimum point on the plot corresponds to the maximum entropy or the population contraction time. Following excitation, the entropy for each initial condition rapidly increases, indicating population dispersion among nearby exciton states on sub-picosecond (ps) timescales. For the core excitations localized in Chl  $a$  509 in CP43 and Chl  $a$  610 in CP47, the ensemble population contracts at 12 ps and 23 ps, respectively (Fig. 2). For excitations in the minor antenna in Chl  $a$  604 in CP26 and Chl  $a$  604 in CP29, the ensemble population contracts at 26 ps and 30 ps, respectively. S-LHCII (B) in the peripheral antenna exhibits population contraction times of 41 ps and 40 ps for respective Chl  $a$  610 and

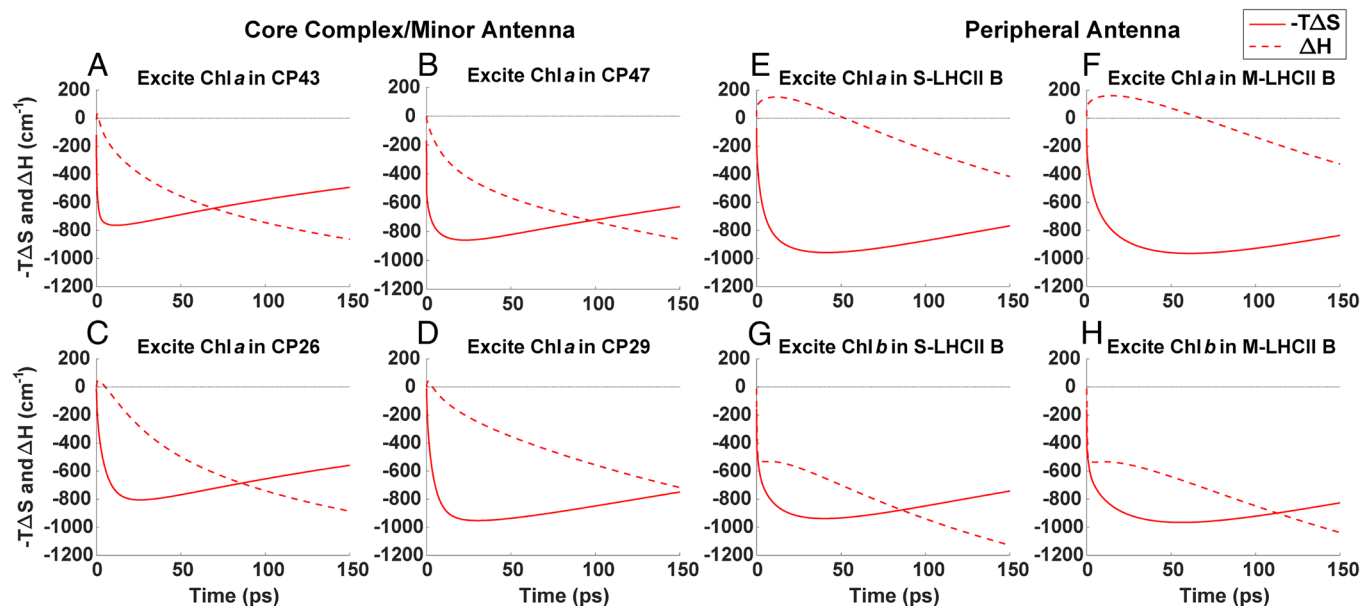


**Fig. 2.** Entropy (solid line) and enthalpy (dashed line) components of the free energy change in time for initial excitations at selected states in the core antenna (A and B), minor antenna (C and D), and peripheral antenna (E–H) complexes. In order of A–E, excitations are localized in Chl *a* 509 in CP43, Chl *a* 610 in CP47, Chl *a* 604 in CP26, Chl *a* 604 in CP29, Chl *a* 610 in S-LHCII (B), Chl *a* 610 in M-LHCII (B), Chl *b* 609 in S-LHCII (B), and Chl *b* 609 in M-LHCII (B).

Chl *b* 609 excitations, while similar excitations in M-LHCII (B) result in 61 ps and 56 ps contraction times.

These times provide insight into the propensity of the initial condition to direct excitations directly toward the RC for trapping or to first spread the excitations out among the pigments. Initial excitations with slower ensemble population contraction toward the RC, and, likewise, a larger contribution from entropy (*SI Appendix, Fig. S3*), are designed to be well connected to many other states. Likewise, states with faster ensemble population contraction times are connected to energetically downhill transfer pathways for more rapid transfer toward the RC.

The enthalpy displays highly variable behavior following excitation in different initial conditions. In some cases, the ensemble population transfers uphill in energy, resulting in an increase in the average enthalpy. For initial excitations in Chl *a* 509 in CP43 (Fig. 2A) and Chl *a* 610 in CP47 (Fig. 2B), this uphill energy transfer is minimal, with the enthalpy maximum occurring within 0.50 ps of initial excitation. Excitations in the minor antenna (Fig. 2 C and D) result in slightly longer-lived uphill EET until 1.30 ps and 0.95 ps for respective excitations in Chl *a* 604 in CP26 and Chl *a* 604 in CP29. For excitations localized in Chl *a*, which account for 214 of the 316 excitations, the entropy term changes much more rapidly than the enthalpy term at early times.

Peripheral Chl *a* excitations (Fig. 2 E and F) result in much longer-lived uphill population transfer. The enthalpy terms for Chl *a* 610 excitations in S-LHCII (B) and M-LHCII (B) maximize at 12 ps and 15 ps, respectively. The maximum enthalpy value, however, is less than 200  $\text{cm}^{-1}$ , or typical thermal energies at room temperature, so this long-lived enthalpy increase is more representative of gradual, rather than energetically steep, uphill energy transfer steps. The states with this long-lived uphill energy transfer tend to be among the lowest-energy states in the complex, but this relationship is not perfectly correlated (*SI Appendix, Fig. S4*). Initial excitations in Chls *a* 610 and 612 of the LHCII (B) complexes display the longest-lasting uphill energy transfer and likewise the longest excitation retention. States with long population retention should provide good candidates for nonphotochemical quenching (NPQ) sites and Chls *a* 610 and 612 in LHCII have previously been suggested to be the sites of NPQ

(36–38). These relatively long-lasting ensemble EET dynamics against an energy gradient also highlight that entropically controlled dynamics do not have to be confined to very short times.

Excitations localized in Chl *b* in the peripheral antenna (Fig. 2 G and H), in contrast, result in exclusively downhill energy transfer in two kinetic phases: first, a rapid (sub-ps) phase followed by a slower (sub-ns) phase toward the RC. The fast timescale likely represents intracomplex equilibration, while the slower component represents intercomplex EET starting around 1 ps.

When both RCs in the PSII dimer are open, the population contraction time for all initial excitations is less than 75 ps, which is about half of the complex's 159 ps fluorescence lifetime, simulated from an initial excitation spread among all Chls *a* in PSII (Fig. 3). There is a general pattern of later population contraction times for states that are more peripheral to the complex, but this is not a very strongly correlated relationship with an  $R^2$  value of 0.68 (*SI Appendix, Fig. S5*). Therefore, the distance of a state from the RC is not sufficient to explain its population contraction time. The trapping time, defined as the mean first passage time for an initial excitation to reach a trap, can provide additional insight into the outcome of an initial excitation. The trapping time is a convolution of the population contraction time and the absolute distance of an excitation from the RC (*SI Appendix, Fig. S11*). When accounting for fluorescence decay (proportional to the transition dipole moment squared, with the average rate for all states set to  $16 \text{ ns}^{-1}$ ) and nonradiative loss (set at  $2 \text{ ns}^{-1}$ ), we find that the probability of trapping in either RC is at least 87% for all initial excitations. To focus on system design principles, we will assume that all population ends up in the traps.

Photosystem II is a symmetric homodimer with two RCs located near the center of the complex and multiple protein subunits holding a fixed number of chlorophyll molecules in consistent orientations (20). When the population contraction times are compared across all PSII excitations, consistencies arise among states in the same protein subunit, particularly the core and minor antenna subunits (*SI Appendix, Fig. S6*). Excitations in the core CP43 subunit next to the D1 protein in the RC have an average population contraction time of 13 ps and a very high (81%) average probability of being trapped in the same-monomer RC (Fig. 4

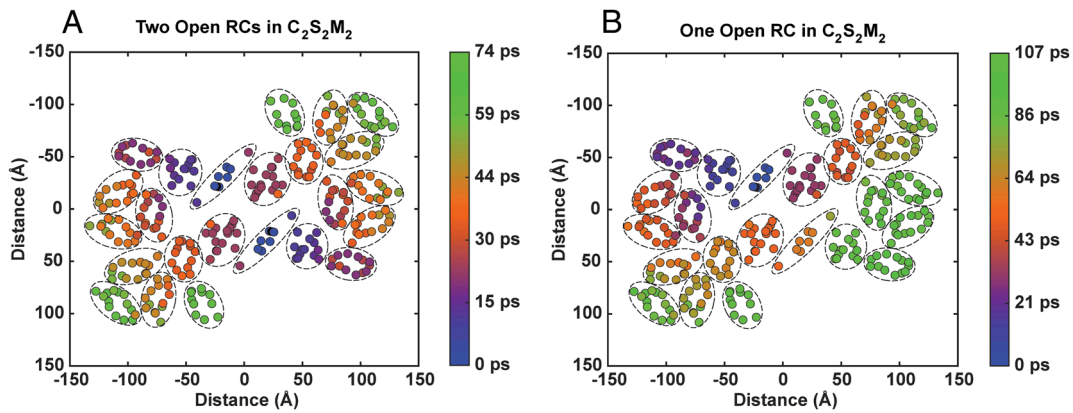


**Fig. 3.** Population contraction times for each initial excitation in the  $C_2S_2M_2$ -type PSII supercomplex when (A) both RCs are open and (B) the monomer 2 (*Bottom*) RC is closed, projected onto the site basis. The charge transfer state is located between  $Chl_{D1}$  and  $Pheo_{D1}$  in the RC.

and *SI Appendix, Fig. S7*). Excitations in the minor antenna CP26 subunit on the same side of the RC, termed the D1 side, have an average population contraction time of 22 ps and a similarly high (80%) average probability of same-monomer RC trapping. In contrast, excitations in the core CP47 subunit next to the D2 protein in the RC have a 24 ps average population contraction time and a 59% average probability of same-monomer trapping. Excitations in the minor antenna CP29 subunit on the same side of the RC, termed the D2 side, have a 33 ps average population contraction time and a 51% average probability of same-monomer trapping.

The faster population contraction times and higher probability of same-monomer trapping on the D1 side subunits (CP43 and CP26) are consistent with experimental and computational observation of faster EET and trapping on the D1 side (13, 27, 39, 40).

The population contraction times among excitations in the S- and M-LHCII trimers are less similar than in the core and minor antenna subunits (Fig. 4 and *SI Appendix, Fig. S7*). For S-LHCII, subunit C, which is closest to CP43 (Fig. 1), has the shortest average contraction time at 28 ps. S-LHCII subunits A and B, meanwhile, display 39 ps and 43 ps respective contraction times. All three S-LHCII subunits (A, B, and C) display high (72, 66, and 71%) probability of trapping in the same-monomer RC, consistent with other D1-side subunits. For M-LHCII, subunits A

and C display similar population contraction times of 45 ps and 47 ps, while subunit B, which is most peripheral (Fig. 1), is slower at 61 ps. All three M-LHCII subunits (A, B, and C) display minimal (46, 49, and 51%) preference for trapping in either monomer RC, consistent with other D2-side subunits.

The faster population contraction times and higher probability of same-monomer trapping for D1-side subunits (CP43, CP26, and S-LHCII) suggest that they are designed to achieve efficient and reliable trapping of excitations. The slower population contraction times and near-agnostic preference for either RC of D2-side subunits (CP47, CP29, and M-LHCII) suggest that they are designed to perform bidirectional energy transfer both toward and away from the same-monomer RC to facilitate intermonomer energy transfer.

The high similarity in the timescales of ensemble population dispersion and contraction among excitations within some protein subunits likely results from rapid intra-subunit equilibration, so interprotein EET dynamics are indifferent to the specific state in the subunit that was excited. Excitations in the core complex (CP43 and CP47) and minor antenna (CP26, CP29, and CP24) subunits have very consistent population contraction times, with SD up to  $\pm 4$  ps. This suggests that these proteins act as distinct units in the PSII energy transfer network. Characterizing each protein's role may help explain the design utility of PSII's distinct subunits, as opposed to a more homogeneous photosystem design like photosystem I (41) or bacterial phycobilisomes (42).

Less similar times of population dispersion and contraction for excitations within the same protein subunit may result from rates of interprotein EET that are comparable to or greater than rates of intraprotein equilibration. The diversity of free energy dynamics among individual states in the LHCII subunits, whose population contraction times have SD up to  $\pm 8$  ps, suggests that this is precisely the case for states in the peripheral antenna.

To further investigate the design of PSII, we consider the free energy terms for another common condition of the system. Natural light levels frequently fluctuate and the RCs of PSII intermittently close as a result of a recent charge separation (1, 33, 43, 44). Fig. 3B demonstrates the population contraction times for each excitation when the RC in monomer 2 (*Bottom*) is closed. The symmetry across the two monomers observed with two open RCs (Fig. 3A) is now broken as excitations cannot be quenched until they encounter the open RC in monomer 1. Even with one closed RC, the slowest population contraction time in the complex is 107 ps, which is less than one-third of the 349 ps computed fluorescence

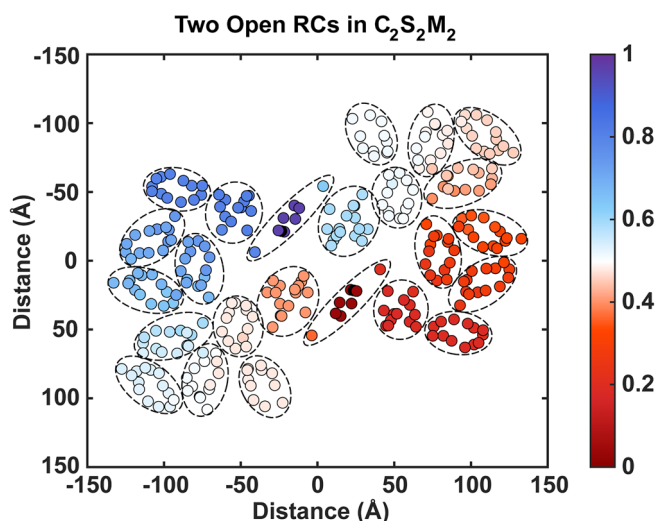


**Fig. 4.** The probability for each initial excitation to be trapped in the monomer 1 RC (*Top*), assuming all population ends up in the traps, projected onto the site basis.

lifetime for a closed monomer 2 RC (Fig. 3B). This means that excitations across both PSII monomers are directed toward the open RC on timescales faster than the fluorescence decay rate, ensuring efficient charge separation is maintained even with one RC closed.

The slowest population contraction times are not observed for the states in the now-closed monomer 2 RC, but rather for states in the D1-side subunits of that RC. The states within the closed RC have population contraction times around 62 ps (SI Appendix, Fig. S8). Excitations in CP47 and CP29 on the D2 side of the closed RC have population contraction times within 50 ps and 65 ps, respectively. In contrast, excitations in CP43 and CP26 on the D1 side of the closed RC have respective population contraction times around 90 ps and 100 ps. Excitations in the S-LCHII subunits in monomer 2 have the slowest population contraction times up to 107 ps when the monomer 2 RC is closed. Meanwhile, the free energy dynamics in the M-LHCII complex on the D2 side of the closed RC are minimally impacted. Evidently, excitations in the D1-side subunits are the most impacted by the closure of the corresponding RC.

The disproportionate elongation of population contraction times for D1-side subunits compared to D2-side subunits of a closed RC further supports the notion that D1-side subunits are designed to perform reliable energy trapping by directing excitations to the RC more quickly. The resilience of D2-side subunit excitations in maintaining relatively fast population contraction times when one RC closes supports the notion that the D2-side subunits are designed to provide many alternative energy transfer pathways for excitations to reach a trap through entropically dominated ensemble dynamics.

Under light stress conditions, the M-LHCII subunits may be removed (45–48), forming the  $C_2S_2$ -type PSII supercomplex, which is the most common form in high light in *Arabidopsis thaliana* (46). Fig. 5 shows the population contraction times for the  $C_2S_2$  supercomplex. With both RCs open, the longest population contraction time is 52 ps, compared to 74 ps for the  $C_2S_2M_2$  supercomplex. When one RC closes, the population contraction times become slightly slower for some states in the  $C_2S_2$  complex, with a 111 ps maximum, than in the larger  $C_2S_2M_2$  complex, with a 107 ps maximum.

For both supercomplexes, the longest population contraction times for the closed monomer-2 RC case occur in the S-LHCII subunit. Returning to our example Chl *a* 610 excitation in S-LHCII (B), we observe population contraction times of 41 ps in  $C_2S_2M_2$  and 42 ps in  $C_2S_2$  when both RCs are open (SI Appendix, Table S1).

When the monomer-2 RC is closed and the same S-LHCII state on the monomer 2 side is excited, these times become 87 ps in  $C_2S_2M_2$  (SI Appendix, Fig. S9) and 101 ps in  $C_2S_2$ , corresponding to times that are respectively 2.1× and 2.4× as long as the two open RCs case. This phenomenon of disproportionate lengthening of population contraction times in  $C_2S_2$  upon an RC closure is also observed for core and minor antenna subunits on the D2 side. For our example Chl *a* 610 excitation in CP47, the ensemble population contracts at 23 ps in  $C_2S_2M_2$  and 12 ps in  $C_2S_2$  when both RCs are open (SI Appendix, Table S1). However, when the monomer 2 RC closes and the same CP47 state in monomer 2 is excited, these times become 49 ps for  $C_2S_2M_2$  and 42 ps for  $C_2S_2$ , which are, respectively, 2× and 3.5× as long as the two open RCs case.

This same pattern is not, however, present for CP43 excitations on the D1 side. Closing the monomer 2 RC results in a Chl *a* 509 excitation in the monomer-2 CP43 subunit displaying population contraction times about 8× and 6× as long as the two open RC case for respective  $C_2S_2M_2$  and  $C_2S_2$  excitations.

If the only role of the M-LHCII complexes is to increase the absorption cross-section for the supercomplex, then the longer population contraction times for  $C_2S_2$  than  $C_2S_2M_2$  following an S-LHCII excitation or a core or minor antenna excitation on the D2 side is an unexpected result, since  $C_2S_2M_2$  clearly has more states for excitations to explore. This result indicates that the M-LHCII complexes play an important role in facilitating intermonomer EET, in line with observations by Yang et al. (12). Not only is intermonomer EET useful to maintain efficient light harvesting in stress conditions, demonstrated by the D2-side subunits when one RC is closed, but it can also serve to increase the efficiency of light harvesting under typical conditions by providing peripheral excitations multiple options to reach a quenching site. This demonstrates the capacity of M-LHCII subunits to create numerous, and potentially more efficient, energy transfer pathways to an open RC that are not present in  $C_2S_2$ .

Clearly, the ability to add and remove LHCII complexes allows PSII to regulate its free energy network, especially the entropy component, by adjusting the number of states that different complexes are connected to (18, 48, 49). Photosynthetic organisms may control the presence of LHCII, and therefore the entropic character of the PSII free energy landscape, to optimize the energy transfer network to their local environment. This work demonstrates the significance of both free energy terms and the ability to regulate them in the design of energy transfer networks.

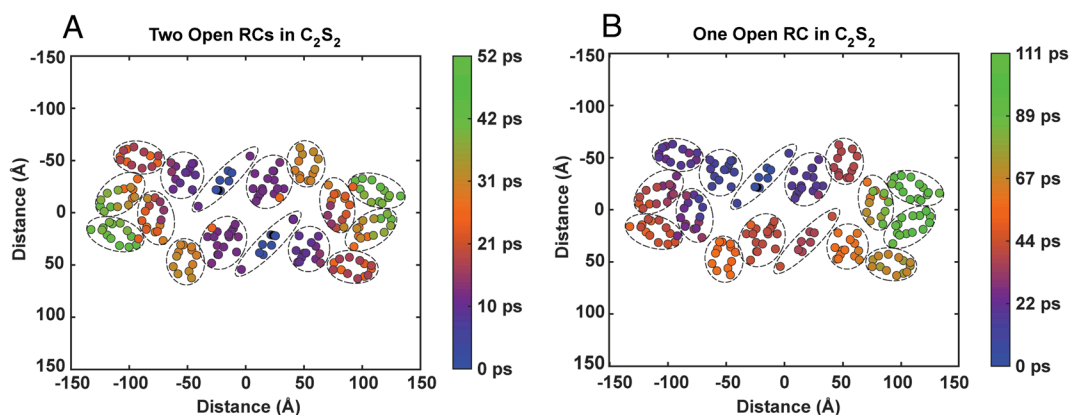


**Fig. 5.** Population contraction times for each initial excitation in the  $C_2S_2$ -type PSII supercomplex when (A) both RCs are open and (B) the monomer 2 (Bottom) RC is closed, projected onto the site basis. The charge transfer state is located between Chl<sub>D1</sub> and Pheo<sub>D1</sub> in the RC.

## Concluding Remarks

In an attempt to understand the design principles underlying the PSII energy transfer network, we studied the free energetics accompanying relaxation of excitations in each state in the PSII supercomplex. The ensemble level calculations described above complement the individual trajectory calculations of Yang et al. (12) and bring a different perspective to the design of the Photosystem II supercomplex. The current calculations show that, at the ensemble level, there are two phases to the motion of excitons: an initial entropy-driven phase in which the ensemble explores the landscape and a second enthalpy-driven phase of more directed motion toward the RC. The first phase can last for up to 50% of the average exciton lifetime, but this component can be modified by the PSII supercomplex via addition or removal of LHCII subunits. Clearly, entropy is being used as a design principle to optimize the structure of the PSII energy transfer network as well as to dynamically respond to different environmental conditions.

We found that the PSII supercomplex contains three primary classes of energy transfer patterns. Some excitations, primarily in D1-side subunits, are well connected to downhill EET steps and display directed transfer toward the trap. Other excitations, particularly in CP47 and CP29 on the D2 side, spread energy out bidirectionally to the RC and periphery. Excitations in the LHCII subunits, particularly M-LHCII, spread energy between the two monomers. Working together, these pathways ensure 1) efficient energy trapping in the RC, 2) effective NPQ in the periphery, and 3) robust energy trapping in the other-monomer RC if the same-monomer RC is closed.

We would not expect to observe these unique features of PSII if its energy landscape were structured as a funnel or as a homogeneous landscape. The variations in connectivity of individual protein subunits makes these different EET patterns possible, demonstrating that employing multiple subunits can provide a selective advantage and even increase quantum efficiency of light harvesting. PSII's dual goals of energy trapping and photoprotection are realized through the varied structure of the free energy network across the complex. States in subunits designed to accomplish reliable energy trapping are engineered to be well-connected

(have fast transfer) to states with lower energy levels in the direction of the RC. To maintain resilience of the energy transfer network, alternative options must be available for trapping, hence the dimeric design of PSII. States designed to maintain PSII energy trapping in varying conditions must be well-connected to many other states, thereby allowing entropy to dominate ensemble dynamics and create diverse energy transfer pathways. Under low-light conditions, PSII can add M-LHCII subunits, which not only expand the light-harvesting capacity of the complex but also increase the connectivity of the two monomers. This illustrates another entropy-motivated design principle in PSII, whereby the complex increases the density of states between the two monomers to promote intermonomer transfer and increase light harvesting rates for certain excitations. As PSII adds and removes LHCII complexes, it is dynamically tuning its entropic landscape, which has significant implications for the energy transfer network. This demonstrates the capacity for entropy to act as a tunable design principle in complex energy transfer systems and illustrates its significance in accomplishing diverse and variable energy transfer goals.

**Data, Materials, and Software Availability.** Data and code data have been deposited in Zenodo (<https://zenodo.org/records/14853026>) (50). All study data are included in the article and/or supporting information. Previously published data were used for this work (The code for constructing the rate matrix is available at: <https://zenodo.org/records/13346121>) (51).

**ACKNOWLEDGMENTS.** This research was supported by the U.S. Department of Energy, Office of Science, Basic Energy Sciences, Chemical Sciences, Geosciences, and Biosciences Division. J.L.H. and S.-J.Y. acknowledge the financial support from the Kavli Energy Nanoscience Institute at Berkeley. D.T.L. is supported by the U.S. Department of Energy, Office of Science, Basic Energy Sciences, CPIMS Program Early Career Research Program under Award DEFOA0002019 and the Alfred P. Sloan Foundation. We thank Doran Raccah for code availability.

Author affiliations: <sup>a</sup>Department of Chemistry, University of California, Berkeley, CA 94720; <sup>b</sup>Molecular Biophysics and Integrated Bioimaging Division, Lawrence Berkeley National Laboratory, Berkeley, CA 94720; <sup>c</sup>Kavli Energy Nanoscience Institute, University of California, Berkeley, CA 94720; <sup>d</sup>Chemical Sciences Division, Lawrence Berkeley National Laboratory, Berkeley, CA 94720; and <sup>e</sup>Materials Sciences Division, Lawrence Berkeley National Laboratory, Berkeley, CA 94720

1. R. E. Blankenship, *Molecular Mechanisms of Photosynthesis* (Wiley, Hoboken, ed. 3, 2022).
2. E. Wientjes, H. Van Amerongen, R. Croce, Quantum yield of charge separation in photosystem II: Functional effect of changes in the antenna size upon light acclimation. *J. Phys. Chem. B* **117**, 11200–11208 (2013).
3. F. Van Mieghem et al., Charge recombination reactions in photosystem II. 1. Yields, recombination pathways, and kinetics of the primary pair. *Biochemistry* **34**, 4798–4813 (1995).
4. P. Müller, X.-P. Li, K. K. Niyogi, Non-photochemical quenching. A response to excess light energy. *Plant Physiol.* **125**, 1558–1566 (2001).
5. J. R. Durrant, L. B. Giorgi, J. Barber, D. R. Klug, G. Porter, Characterisation of triplet states in isolated photosystem II reaction centres: Oxygen quenching as a mechanism for photodamage. *Biochim. Biophys. Acta Bioenerg.* **1017**, 167–175 (1990).
6. A. Krieger-Liszkay, Singlet oxygen production in photosynthesis. *J. Exp. Bot.* **56**, 337–346 (2004).
7. A. V. Ruban, Nonphotochemical chlorophyll fluorescence quenching: Mechanism and effectiveness in protecting plants from photodamage. *Plant Physiol.* **170**, 1903–1916 (2016).
8. H. Ishikita, B. Loll, J. Biesiadka, W. Saenger, E.-W. Knapp, Redox potentials of chlorophylls in the photosystem II reaction center. *Biochemistry* **44**, 4118–4124 (2005).
9. B. Genty, J.-M. Briantais, N. R. Baker, The relationship between the quantum yield of photosynthetic electron transport and quenching of chlorophyll fluorescence. *Biochim. Biophys. Acta Gen. Subj.* **990**, 87–92 (1989).
10. A. V. Ruban, S. Wilson, The mechanism of non-photochemical quenching in plants: Localization and driving forces. *Plant Cell Physiol.* **62**, 1063–1072 (2021).
11. T. Mirkovic et al., Light absorption and energy transfer in the antenna complexes of photosynthetic organisms. *Chem. Rev.* **117**, 249–293 (2017).
12. S.-J. Yang, D. J. Wales, E. J. Woods, G. R. Fleming, Design principles for energy transfer in the photosystem II supercomplex from kinetic transition networks. *Nat. Commun.* **15**, 8763 (2024).
13. C. Leonardo et al., Bidirectional energy flow in the photosystem II supercomplex. *J. Phys. Chem. B* **128**, 7941–7953 (2024).
14. R. C. Jennings et al., A study of photosystem II fluorescence emission in terms of the antenna chlorophyll-protein complexes. *Biochim. Biophys. Acta Bioenerg.* **1183**, 194–200 (1993).
15. R. C. Jennings, R. Bassi, F. M. Garlaschi, P. Dainese, G. Zucchelli, Distribution of the chlorophyll spectral forms in the chlorophyll-protein complexes of photosystem II antenna. *Biochemistry* **32**, 3203–3210 (1993).
16. D. I. G. Bennett, K. Amarnath, G. R. Fleming, A structure-based model of energy transfer reveals the principles of light harvesting in photosystem II supercomplexes. *J. Am. Chem. Soc.* **135**, 9164–9173 (2013).
17. Y. Shibata, S. Nishi, K. Kawakami, J.-R. Shen, T. Renger, Photosystem II does not possess a simple excitation energy funnel: Time-resolved fluorescence spectroscopy meets theory. *J. Am. Chem. Soc.* **135**, 6903–6914 (2013).
18. R. Croce, H. Van Amerongen, Natural strategies for photosynthetic light harvesting. *Nat. Chem. Biol.* **10**, 492–501 (2014).
19. X. Wei et al., Structure of spinach photosystem II-LHCII supercomplex at 3.2 Å resolution. *Nature* **534**, 69–74 (2016).
20. X. Su et al., Structure and assembly mechanism of plant C2 S2 M2-type PSII-LHCII supercomplex. *Science* **357**, 815–820 (2017).
21. M. Ballottari, J. Girardon, L. Dall'Osto, R. Bassi, Evolution and functional properties of photosystem II light harvesting complexes in eukaryotes. *Biochim. Biophys. Acta Bioenerg.* **1817**, 143–157 (2012).
22. E. J. Boekema, H. Van Roon, F. Calkoen, R. Bassi, J. P. Dekker, Multiple types of association of photosystem II and its light-harvesting antenna in partially solubilized photosystem II membranes. *Biochemistry* **38**, 2233–2239 (1999).
23. E. J. Boekema, H. Van Roon, J. F. L. Van Breemen, J. P. Dekker, Supramolecular organization of photosystem II and its light-harvesting antenna in partially solubilized photosystem II membranes. *Eur. J. Biochem.* **266**, 444–452 (1999).
24. S. Caffari, R. Kouřil, S. Kereiche, E. J. Boekema, R. Croce, Functional architecture of higher plant photosystem II supercomplexes. *EMBO J.* **28**, 3052–3063 (2009).
25. A. Crepin, S. Caffari, Functions and evolution of Lhcb isoforms composing LHCII, the major light harvesting complex of photosystem II of green eukaryotic organisms. *CPPS* **19**, 699–713 (2018).
26. J. P. Dekker, E. J. Boekema, Supramolecular organization of thylakoid membrane proteins in green plants. *Biochim. Biophys. Acta Bioenerg.* **1706**, 12–39 (2005).

27. G. Raszewski, T. Renger, Light harvesting in photosystem II core complexes is limited by the transfer to the trap: Can the core complex turn into a photoprotective mode? *J. Am. Chem. Soc.* **130**, 4431–4446 (2008).
28. G. Raszewski, W. Saenger, T. Renger, Theory of optical spectra of photosystem II reaction centers: Location of the triplet state and the identity of the primary electron donor. *Biophys. J.* **88**, 986–998 (2005).
29. F. Müh, M.E.-A. Madjet, T. Renger, Structure-based simulation of linear optical spectra of the CP43 core antenna of photosystem II. *Photosynth. Res.* **111**, 87–101 (2012).
30. V. Mascoli, V. Novoderezhkin, N. Liguori, P. Xu, R. Croce, Design principles of solar light harvesting in plants: Functional architecture of the monomeric antenna CP29. *Biochim. Biophys. Acta Bioenerg.* **1861**, 148156 (2020).
31. V. Novoderezhkin, A. Marin, R. Van Grondelle, Intra- and inter-monomeric transfers in the light harvesting LHCII complex: The Redfield–Förster picture. *Phys. Chem. Chem. Phys.* **13**, 17093 (2011).
32. M. Yang, G. R. Fleming, Influence of phonons on exciton transfer dynamics: Comparison of the Redfield, Förster, and modified Redfield equations. *Chem. Phys.* **275**, 355–372 (2002).
33. K. Amarnath, D. I. G. Bennett, A. R. Schneider, G. R. Fleming, Multiscale model of light harvesting by photosystem II in plants. *Proc. Natl. Acad. Sci. U.S.A.* **113**, 1156–1161 (2016).
34. D. T. Limmer, *Statistical Mechanics and Stochastic Thermodynamics: A Textbook on Modern Approaches in and out of Equilibrium* (Oxford University Press, Oxford, 2024).
35. H. H. Nguyen *et al.*, Charge separation in the photosystem II reaction center resolved by multispectral two-dimensional electronic spectroscopy. *Sci. Adv.* **9**, eade7190 (2023).
36. A. V. Ruban, F. Saccon, Chlorophyll a de-excitation pathways in the LHCII antenna. *J. Chem. Phys.* **156**, 070902 (2022).
37. R. Van Grondelle, V. I. Novoderezhkin, Energy transfer in photosynthesis: Experimental insights and quantitative models. *Phys. Chem. Chem. Phys.* **8**, 793–807 (2006).
38. A. V. Ruban *et al.*, Identification of a mechanism of photoprotective energy dissipation in higher plants. *Nature* **450**, 575–578 (2007).
39. S.-J. Yang *et al.*, From antenna to reaction center: Pathways of ultrafast energy and charge transfer in photosystem II. *Proc. Natl. Acad. Sci. U.S.A.* **119**, e2208033119 (2022).
40. F. L. De Weerd, I. H. M. Van Stokkum, H. Van Amerongen, J. P. Dekker, R. Van Grondelle, Pathways for energy transfer in the core light-harvesting complexes CP43 and CP47 of photosystem II. *Biophys. J.* **82**, 1586–1597 (2002).
41. B. Gobets, R. Van Grondelle, Energy transfer and trapping in photosystem I. *Biochim. Biophys. Acta Bioenerg.* **1507**, 80–99 (2001).
42. S. Sohoni *et al.*, Phycobilisome's exciton transfer efficiency relies on an energetic funnel driven by chromophore-linker protein interactions. *J. Am. Chem. Soc.* **145**, 11659–11668 (2023).
43. G. Sipka *et al.*, Light-adapted charge-separated state of photosystem II: Structural and functional dynamics of the closed reaction center. *Plant Cell* **33**, 1286–1302 (2021).
44. R. A. Slattery, B. J. Walker, A. P. M. Weber, D. R. Ort, The impacts of fluctuating light on crop performance. *Plant Physiol.* **176**, 990–1003 (2018).
45. P. Horton, Optimization of light harvesting and photoprotection: Molecular mechanisms and physiological consequences. *Philos. Trans. R. Soc. B* **367**, 3455–3465 (2012).
46. P. Albanese *et al.*, Dynamic reorganization of photosystem II supercomplexes in response to variations in light intensities. *Biochim. Biophys. Acta Bioenerg.* **1857**, 1651–1660 (2016).
47. R. Kouřil, E. Wientjes, J. B. Bultema, R. Croce, E. J. Boekema, High-light vs. low-light: Effect of light acclimation on photosystem II composition and organization in *Arabidopsis thaliana*. *Biochim. Biophys. Acta Bioenerg.* **1827**, 411–419 (2013).
48. R. Croce, Beyond 'seeing is believing': The antenna size of the photosystems in vivo. *New Phytol.* **228**, 1214–1218 (2020).
49. S. Caffari, K. Broess, R. Croce, H. Van Amerongen, Excitation energy transfer and trapping in higher plant photosystem II complexes with different antenna sizes. *Biophys. J.* **100**, 2094–2103 (2011).
50. J. L. Hall, S.-J. Yang, D. T. Limmer, G. R. Fleming, Data and code for "Entropy as a design principle in the photosystem II supercomplex". Zenodo. <https://zenodo.org/records/14853026>. Deposited 16 December 2024.
51. S.-J. Yang, D. J. Wales, E. J. Woods, G. R. Fleming, Data and code for "Design principles for energy transfer in the photosystem II supercomplex from kinetic transition networks". Zenodo. <https://zenodo.org/records/13346121>. Deposited 22 August 2024.